

AD 740576

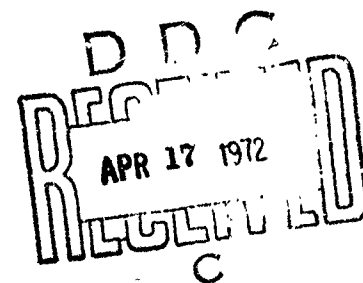
AFRL-72-0047
17 JANUARY 1972
PHYSICAL SCIENCES RESEARCH PAPERS, NO. 474



AIR FORCE CAMBRIDGE RESEARCH LABORATORIES
L. G. HANSCOM FIELD, BEDFORD, MASSACHUSETTS

Scattering of HF Radio Waves by Elliptical Electron Density Distributions

**VICTOR L. CORBIN
MILTON M. KLEIN**



Approved for public release; distribution unlimited.

NATIONAL TECHNICAL
INFORMATION SERVICE

AIR FORCE SYSTEMS COMMAND
United States Air Force



Unclassified
Security Classification

DOCUMENT CONTROL DATA - R&D		
<i>(Security classification of title, body of abstract and indexing annotation must be entered when the overall report is classified)</i>		
1. ORIGINATING ACTIVITY (Corporate author) Air Force Cambridge Research Laboratories (LKC) L.G. Hanscom Field Bedford, Massachusetts 01730		2a. REPORT SECURITY CLASSIFICATION Unclassified
		2b. GROUP
3. REPORT TITLE SCATTERING OF HF RADIO WAVES BY ELLIPTICAL ELECTRON DENSITY DISTRIBUTIONS		
4. DESCRIPTIVE NOTES (Type of report and inclusive dates) Scientific. Interim.		
5. AUTHOR(S) (First name, middle initial, last name) Victor L. Corbin Milton M. Klein		
6. REPORT DATE 17 January 1972	7a. TOTAL NO. OF PAGES 42	7b. NO. OF REFS 11
8a. CONTRACT OR GRANT NO.	9a. ORIGINATOR'S REPORT NUMBER(S) AFCRL-72-0047	
a. PROJECT, TASK, WORK UNIT NOS. 7635-13-01		
c. DOD ELEMENT 62101F		
d. DOD SUBELEMENT 681000	9b. OTHER REPORT NO(S) (Any other numbers that may be assigned this report) PSRP No. 474	
10. DISTRIBUTION STATEMENT Approved for public release; distribution unlimited.		
11. SUPPLEMENTARY NOTES TECH, OTHER	12. SPONSORING MILITARY ACTIVITY Air Force Cambridge Research Laboratories (LKC) L.G. Hanscom Field Bedford, Massachusetts 01730	
13. ABSTRACT The differential and total cross sections for ellipsoids and elliptic cylinders having Gaussian electron density distributions have been obtained by a ray tracing procedure. Calculations for the case of an external magnetic field were restricted to the ellipsoidal distributions. The results show that the scattering is extremely sensitive to the orientation of the body. A peak in cross section occurs at the scattering angle corresponding to the ray normal to the critical surface, and increases as the surface becomes flatter. The cross section is sensitive to the ratio of peak density to critical density for moderate values but becomes relatively insensitive when the ratio exceeds 3. The total cross section is a very sensitive function of both orientation and ratio of major to minor axes. The introduction of a magnetic field decreases the ordinary ray cross section; the extraordinary ray exhibits higher values only in the forward scattering region, but is always higher for the spherical case. Comparison of the Gaussian ellipsoid with the corresponding conducting ellipsoid shows that the Gaussian has a large cross section in the forward region but considerably lower values in the backscatter region.		

DD FORM 1473
NOV 65

Unclassified
Security Classification

Unclassified
Security Classification

14. KEY WORDS	LINK A		LINK B		LINK C	
	ROLE	WT	ROLE	WT	ROLE	WT
Scattering Magnetic field Radio waves Charge distribution Ray optics						

Unclassified
Security Classification

AFCRL-72-0047
17 JANUARY 1972
PHYSICAL SCIENCES RESEARCH PAPERS, NO. 474



AERONAUTICAL LABORATORY PROJECT 7635

AIR FORCE CAMBRIDGE RESEARCH LABORATORIES

L. G. HANSCOM FIELD, BEDFORD, MASSACHUSETTS

Scattering of HF Radio Waves by Elliptical Electron Density Distributions

**VICTOR L. CORBIN
MILTON M. KLEIN**

Approved for public release; distribution unlimited.

**AIR FORCE SYSTEMS COMMAND
United States Air Force**

Abstract

The differential and total cross sections for ellipsoids and elliptic cylinders having Gaussian electron density distributions have been obtained by a ray tracing procedure. Calculations for the case of an external magnetic field were restricted to the ellipsoidal distributions. The results show that the scattering is extremely sensitive to the orientation of the body. A peak in cross section occurs at the scattering angle corresponding to the ray normal to the critical surface, and increases as the surface becomes flatter. The cross section is sensitive to the ratio of peak density to critical density for moderate values but becomes relatively insensitive when the ratio exceeds 3. The total cross section is a very sensitive function of both orientation and ratio of major to minor axes. The introduction of a magnetic field decreases the ordinary ray cross section; the extraordinary ray exhibits higher values only in the forward scattering region, but is always higher for the spherical case. Comparison of the Gaussian ellipsoid with the corresponding conducting ellipsoid shows that the Gaussian has a large cross section in the forward region but considerably lower values in the backscatter region.

Contents

1. INTRODUCTION	1
2. ANALYSIS	2
3. PROCEDURE	3
4. RESULTS FOR A LONG CYLINDER	7
5. RESULTS FOR THE PROLATE ELLIPSOID	16
6. RESULTS OF THE PROLATE ELLIPSOID IN A MAGNETIC FIELD	18
7. COMPARISON OF GAUSSIAN AND CONDUCTING ELLIPSOIDS	19
8. CONCLUDING REMARKS	21
APPENDIX A—Computer Code for Ellipsoidal Scattering	23
REFERENCES	37

Illustrations

1. Geometry and Coordinate System of the Electron Density Distribution	4
2. Scattering From an Elliptic Cylinder with $\rho = 2.0$, $R_0 = 3$, and $\theta_R = 0^\circ$	8
3. Scattering From an Elliptic Cylinder with $\rho = 2.0$, $R_0 = 3$, and $\theta_R = 45^\circ$	9
4. Scattering From an Elliptic Cylinder with $\rho = 2.0$, $R_0 = 3$, and $\theta_R = 90^\circ$	10
5. Differential Cross Section for $\rho = 2.0$, $\theta_R = 0^\circ$, and Several Values of R_0	11
6. Differential Cross Section for $\rho = 2.0$, $\theta_R = 45^\circ$, and Several Values of R_0	12
7. Differential Cross Section for $\rho = 2.0$, $\theta_R = 90^\circ$, and Several Values of R_0	13
8. Angle of Relative Maximum of Differential Cross Section vs θ_R	14
9. Total Cross Section vs ρ for $R_0 = 3$, and Several Values of θ_R	15
10. Total Cross Section vs R_0 for $\rho = 2.0$, and Several Values of θ_R	15
11. Total Cross Section vs θ_R for $\rho = 2.0$, and Several Values of R_0	16
12. Differential Cross Section vs Scattering Angle with Azimuthal Symmetry, $\rho = 2.0$, $\theta_R = 0^\circ$, and Several Values of R_0	17
13. Total Cross Section of Ellipsoid vs R_0 for $\theta_R = 0^\circ$ and $\rho = 2.0$	18
14. Differential Cross Section of Ordinary Ray vs Scattering Angle for $\rho = 2.0$, $\theta_R = 0^\circ$, and Several Values of R_0	19
15. Differential Cross Section of Extraordinary Ray vs Scattering Angle for $\rho = 2.0$, $\theta_R = 0^\circ$, and Several Values of R_0	20
16. Comparison of Conducting Ellipsoid and Ellipsoidal Electron Density Distribution	21

Scattering of HF Radio Waves by Elliptical Electron Density Distributions

1. INTRODUCTION

In recent years there has been some work performed on the scattering of High Frequency (HF) radio waves by artificial charge distributions in the ionosphere. The most notable of these are the "SECEDE" Barium Releases which have been discussed in the literature (Bates, 1971; Rao, et al., 1971; Thome, 1969). Up to this time, there has not been a thorough investigation into the scattering by these releases as a function of angle of the incident wave to the major axis of the releases.

We have therefore calculated the total cross section and the differential cross section of a long cylindrical charge distribution with an ellipsoidal cross section and a two-dimensional Gaussian electron density distribution for several orientations of the major axis of the distribution to the incident wave. To perform these calculations we apply the theory of ray optics and use Macgregor's differential equations (Kelso, 1964) to calculate the ray paths. To calculate the index of refraction, we have employed the Appleton-Hartree dispersion equation (Kelso, 1964) neglecting absorption by the medium.

In the following discussion, we will present our results for the differential and total cross section of long cylindrical bodies which have various ellipsoidal cross sections and differing electron contents. In addition, we will treat the case of a

(Received for publication 17 January 1972)

prolate ellipsoid when the direction of propagation of the incident wave is along the major axis of the ellipsoid.

Although it is known that the artificially induced charge distributions take an ellipsoidal form, we will initially treat the simpler case of an infinitely long cylinder with an elliptic cross section. The special case of the incident plane wave parallel to the major axis of the charge distribution can be treated as a prolate ellipsoid since there is no dependence on azimuthal angle, and thus the cross section is a function of scattering angle only. The azimuthal dependence of the cross section, which is important in the case of an incident wave at an oblique angle to the charge distribution, has not been included in our calculations.

2. ANALYSIS

For a spherically symmetric distribution the scattering cross section is given by the formula (Merzbacher, 1961)

$$\sigma(\theta) = \frac{4\pi b}{\sin \theta} \left| \frac{db}{d\theta} \right| \quad (1)$$

where b is the impact parameter, and θ the scattering angle. We have introduced a factor of 4π in order to be consistent with the definition used in radar cross section studies.

A more general formula (Merzbacher, 1961) for the differential cross section is

$$dA = \sigma(\Omega) dA' \quad (2)$$

where dA is the incident flux per unit area and dA' the area into which it is scattered.

For a long cylinder, neglecting end effects,

$$dA = db dy \quad (3)$$

where b is the impact parameter and y is a length along the cylinder. In cylindrical coordinates, we have

$$\sigma(\Omega) dA' = \sigma(\theta, y) d\theta dy \quad (4)$$

where θ is the scattering angle. Substituting Eqs. (3) and (4) into Eq. (2),

$$db dy = \sigma(\theta, y) d\theta dy. \quad (5)$$

Since the cylinder has a uniform cross sectional area along its length, σ is a function only of θ , and we can thus integrate the y component to obtain

$$db = \sigma(\theta)d\theta. \quad (5)$$

Introducing the factor of 2π to be consistent with radar cross sections, we obtain

$$\sigma(\theta) = 2\pi \left| \frac{db}{d\theta} \right|. \quad (7)$$

Eq. (7) was used to calculate the differential cross section per unit length of the cylinder. For convenience, we have taken the unit of length to be 1 km. The total cross section can be calculated by integrating the above equation over θ .

In order to evaluate the derivative in Eq. (1), we must calculate the paths of a number of rays in order to obtain the dependence of b on θ . These ray paths are determined by Haselgrove's equations, which we will discuss in the next section. The evaluation of the derivative was worked out with the help of Rosenberg (Rosenberg, 1971), who has written a spline fitting program (Ahlberg, 1967) which allows us to fit a function to a number of cubic polynomials so that the first derivative is continuous or nearly continuous at each point along the curve. Thus we can calculate $\sigma(\theta)$ under a variety of different conditions.

3. PROCEDURE

We now discuss the evaluation of Haselgrove's equations and the computer code which was written to calculate the scattering cross section of a long cylinder with an ellipsoidal cross section. Figure 1 shows the system of coordinates which we have used in our analysis. The x -axis is horizontal, the z -axis is in the vertical plane, and the y -axis points into the paper. The rotation angle of the ellipse θ_R is measured counterclockwise from the positive x -axis to the major axis of the ellipse. The impact parameter b is measured from the x -axis and is incident from the left. The perimeter of the ellipse is the curve along which, when no magnetic field is present, the index of refraction $\mu(x,z)$ is zero (critical ellipse). The distance Z is the z -coordinate of the point in the left-hand plane, where the tangent to the ellipse is perpendicular to the x -axis.

In order to solve Eq. (7), a Fortran computer program was written to calculate $b(\theta)$ and subsequently evaluate $\sigma(\theta)$ for a number of different parameters. Following is a brief description of the steps involved in the computations. Appendix A contains a copy of the computer code which was written.

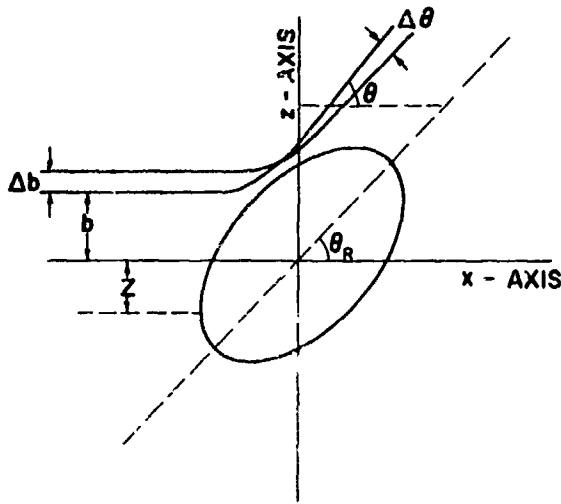


Figure 1. Geometry and Coordinate System of the Electron Density Distribution

The first step in the calculation of cross section is the determination of the rays which define $b(\theta)$. In order to calculate the rays, we need a set of impact parameters which should cover the complete range of scattering angles. This set of impact parameters varies according to the orientation and width of the cylinder. To determine a complete set of impact parameters, we calculate a quantity Z' about which we symmetrically distribute the impact parameters by

$$Z' = Z - .3 \sin(\theta_R) Z_{\max} \quad (8)$$

where θ_R is the angle the major axis makes with the x-axis, and Z_{\max} is the maximum z coordinate of the critical ellipse. The above empirical formula was found to work sufficiently well for the rotation angles 0° , 45° and 90° .

The impact parameters were closely spaced near the value of Z' , but the spacing increases as we proceeded away from the line of symmetry. The maximum separation between impact parameters was .25 km, and they extended to a distance of $4 Z_{\max}$ from Z .

Once we have chosen the impact parameters, we launch each ray from an x coordinate of -5 km towards the ellipse. Haselgrove's equations, which define the path that a ray will take in a medium with an index of refraction μ are:

$$\begin{aligned} \frac{\partial x}{\partial t} &= \frac{c}{\mu^2} (\mu \cos \alpha + \frac{\partial \mu}{\partial \alpha} \sin \alpha) \\ \frac{\partial z}{\partial t} &= \frac{c}{\mu^2} (\mu \sin \alpha - \frac{\partial \mu}{\partial \alpha} \sin \alpha) \\ \frac{\partial \alpha}{\partial t} &= \frac{c}{\mu^2} (\cos \alpha \frac{\partial \mu}{\partial z} - \sin \alpha \frac{\partial \mu}{\partial x}) \end{aligned} \quad (9)$$

where $\mu(x,z)$ is the index of refraction at the point (x,z) . The phase angle of the ray is α , and $\frac{dz}{dx}$ is the angle between the ray direction and the initial direction of

propagation. To solve Haselgrove's equations by computer techniques, Eqs. (9) were transformed into Eqs. (10),

$$\begin{aligned}\Delta x &= \Delta d \left(\mu \cos \alpha + \frac{\partial \mu}{\partial \alpha} \sin \alpha \right) / \mu^2 \\ \Delta z &= \Delta d \left(\mu \sin \alpha - \frac{\partial \mu}{\partial \alpha} \cos \alpha \right) / \mu^2 \\ \Delta \alpha &= \Delta d \left(\cos \alpha \frac{\partial \mu}{\partial z} - \sin \alpha \frac{\partial \mu}{\partial x} \right) / \mu^2\end{aligned}\quad (10)$$

where $\Delta d = c \Delta t$ and c is the speed of light. The quantity Δd which was used in integrating the above equations represents the step size which at a maximum was 0.5 km. This value was decreased by the program such that in no step would the phase angle change by more than 3° . The integration was carried out by means of a Runge-Kutta method for the solution of a set of simultaneous linear differential equations (Scarborough, 1930). When the calculation of the rays was performed with a step size of 0.25 km, half the normal step size, the maximum difference in the scattering angle was 0.009° . The difference in the scattering cross section was less than 0.001 km^2 where the maximum scattering error occurred.

The value of μ at each point that the equations were evaluated is given by the Appleton-Hartry Dispersion Equation,

$$\mu^2(x, z) = 1 - \frac{X(1 - Y^2)}{1 - X - \frac{Y_t^2}{2} \pm \sqrt{\frac{Y_t^2}{4} + Y_l^2 (1 - X)^2}} \quad (11)$$

where

$$X(x, z) = \rho \exp \left[- \left(\frac{x^2}{x_0^2} + \frac{z^2}{z_0^2} \right) \right]. \quad (12)$$

A measure of the hardness of the charge distribution is ρ , which is defined as the ratio of peak plasma density to the critical plasma density. If ρ is somewhat greater than 1, we have a hard charge distribution, for which we consequently have a significant region of backscatter.

The Gaussian half widths of the charge distributions are x_0 and z_0 .

The gyromagnetic ratio (ratio of ion frequency/incident frequency) is Y , and Y_t and Y_l are the transverse and longitudinal components of the gyromagnetic ratio,

$$\begin{aligned}
 Y_t &= Y \sin (\alpha - \theta_H) \\
 Y_l &= Y \cos (\alpha - \theta_H)
 \end{aligned}
 \tag{13}$$

where θ_H is the angle the magnetic field makes with the incident wave. In the case of a nonmagnetic field, $Y = 0$, and the equation for the index of refraction simplifies to

$$\mu^2(x, z) = 1 - X.
 \tag{14}$$

Once each impact parameter has traced a ray, the resulting table of b and θ define $b(\theta)$.

The value of b for $\theta = 180^\circ$ is defined as the displacement, and it is subtracted from all values of b . The reason for the displacement is the asymmetry of an elliptical charge distribution when it is rotated with respect to the incident plane wave, or when a magnetic field is present.

The table of b and θ is then interpolated at intervals of 1° with a cubic spline, and the slope at each point is calculated. Since the slope has a few discontinuities due to imperfections in the method of interpolation, it is smoothed by taking an 11 point running average twice.

The process of smoothing is of questionable value since the total cross sections appear to be increased by as much as 10% when the smooth data is used. The effect of smoothing appears to "lift" the curve, thus increasing the value of the integral. The region where the smoothing is needed is normally in the backscatter region where the cross section is small. Thus it would seem that, although not aesthetically pleasing, the curves with small discontinuities in the backscatter region are more accurate over the completed range of angles than the smoothed curves.

Once we have the derivative, the cross section is easily calculated by Eq. (7), and the total cross section

$$\sigma = \int_0^{2\pi} \left| \frac{db}{d\theta} \right| d\theta.
 \tag{15}$$

The values at 0° and 360° are determined by linear extrapolation.

In order to compare the cross section values to a cylindrical rod of circular cross section, we have calculated the values of x_0 and z_0 such that the total electron content in a slice of the cylinder is the same.

The electron content in a circular cylinder of unit length is

$$\int_{-\infty}^{\infty} \int_{-\infty}^{\infty} \rho \exp\left(-\frac{x^2+z^2}{r_0^2}\right) dx dz = \rho \pi r_0^2, \quad (16)$$

and the electron content in an ellipsoidal cylinder of unit length is

$$\int_{-\infty}^{\infty} \int_{-\infty}^{\infty} \rho \exp\left(-\frac{x^2}{x_0^2} - \frac{z^2}{z_0^2}\right) dx dz = \rho \pi x_0 z_0. \quad (17)$$

Therefore the electron content for a slice of a cylinder will remain constant if the product of the major and minor axes remains constant.

If we take $r_0 = 1$ km, then

$$1 = x_0 z_0. \quad (18)$$

If we want an ellipse with $x_0/z_0 = 5 = R_0$, then

$$1 = 5z_0^2. \quad (19)$$

We will now be able to determine not only how the orientation of the charge distribution changes the cross sections, but how the shape of the distribution affects the cross section.

The program which was written had a number of parameters which could be changed to investigate their effects on the cross section. These parameters were ρ , x_0 , z_0 and θ_R . The output of the program was: impact parameters, the total cross section per unit length, and a tabulation of b , $db/d\theta$, $\sigma(\theta)$ at 1° intervals, and total cross section.

4. RESULTS FOR A LONG CYLINDER

The program to calculate the cross sections produces 6 graphs for each choice of parameters. The curves are the ray paths (Figures 2a, 3a, 4a), the function $f(\theta)$ (Figures 2b, 3b, 4b), the derivative $db/d\theta$ (Figures 2c, 3c, 4c), and the cross section (Figures 2d, 3d, 4d). In addition, the smooth values of derivative and cross section are also plotted but are not shown. Figure 2 has the ellipse unrotated, Figure 3 has the ellipse rotated 45° , and Figure 4 has the ellipse rotated 90° . In all three cases, $\rho = 2$ and $R_0 = 3$. In Figures 5, 6, 7 we have shown the differential cross section for $R_0 = 1, 2, \text{ and } 5$; $\theta_R = 0, 45^\circ \text{ and } 90^\circ$ with $\rho = 2.0$.

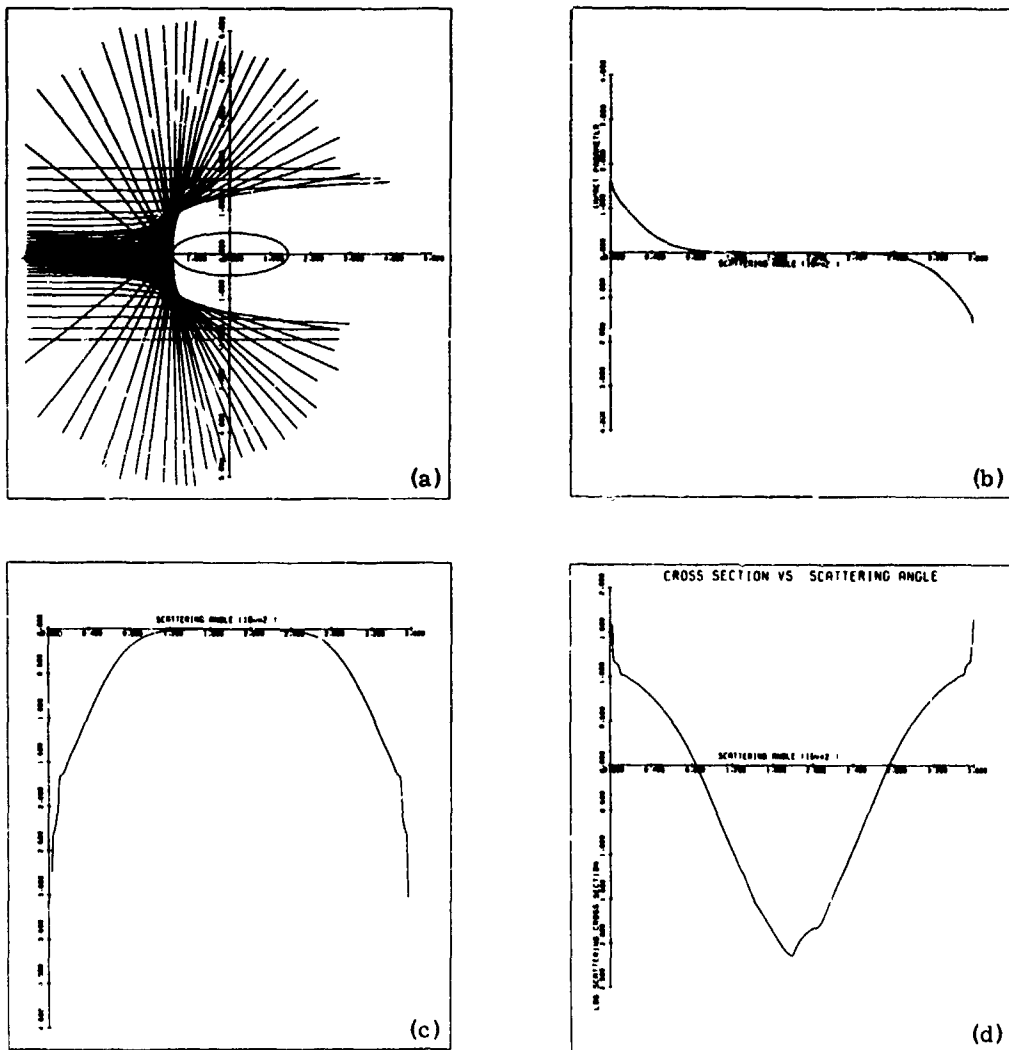


Figure 2. Scattering From an Elliptic Cylinder with $\rho = 2.0$, $R_0 = 3$, and $\theta_R = 0^\circ$; (a) Ray Paths, (b) b vs θ , (c) $db/d\theta$, (d) $\sigma(\theta)$

From the figures, it can be seen how the detail structure varies with different orientations, and the sharp peak when R_0 is largest.

If we carefully examine the differential cross section curves in Figures 6 and 7, we notice that the cross section reaches a relative maximum between the end points. This peak, which is dependent on the angle between the major axis of the ellipse and the propagation direction, increases the total cross section. The radius of curvature of the charge distribution is also an important factor. The peak is highest when the curvature is small, and the wave normal is perpendicular to the tangent of the charge distribution at the point of contact with the critical surface.

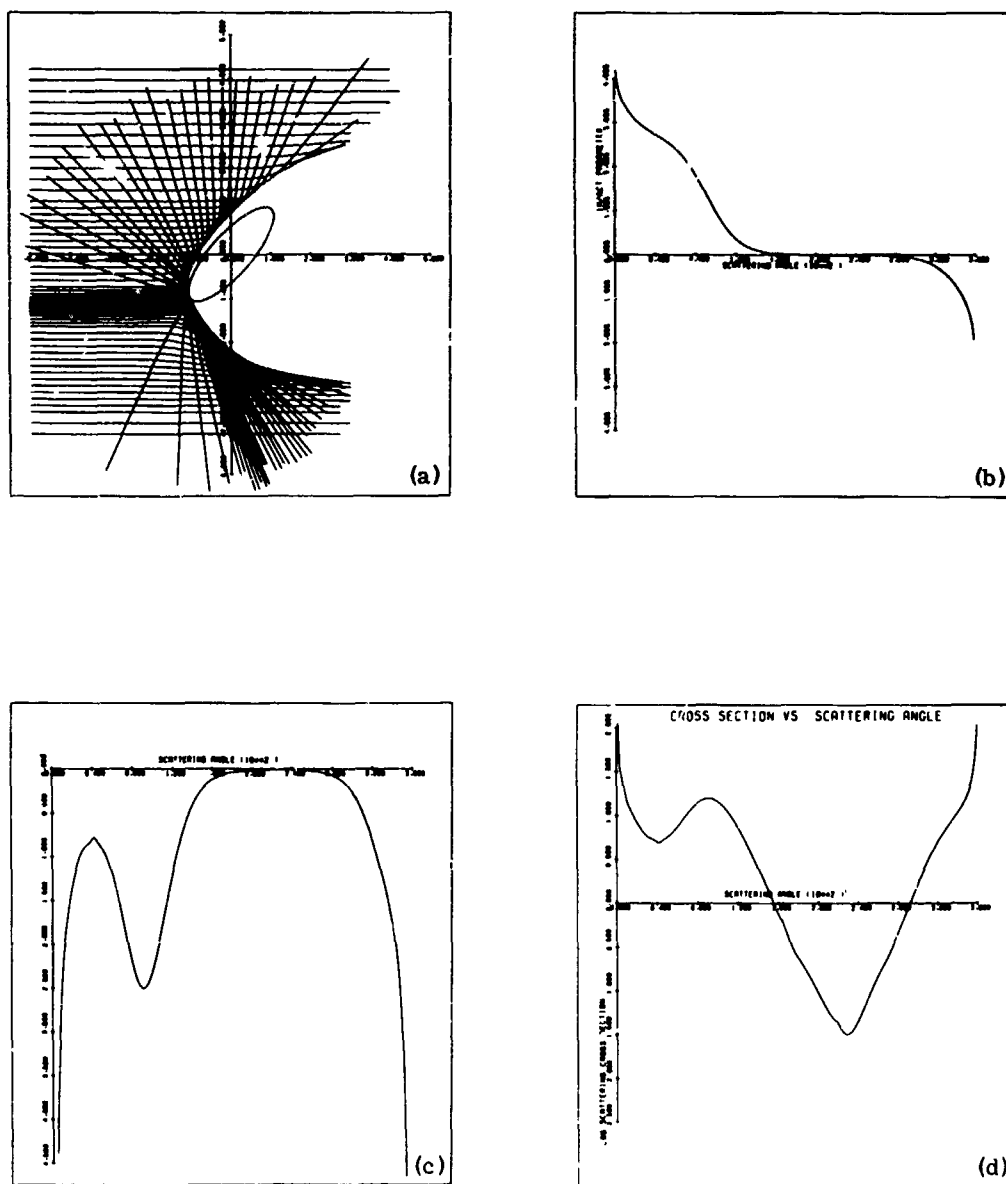


Figure 3. Scattering From an Elliptic Cylinder with $\rho = 2.0$, $R_0 = 3$, and $\theta_R = 45^\circ$;
 (a) Ray Paths, (b) b vs θ , (c) $db/d\theta$, (d) $\sigma(\theta)$

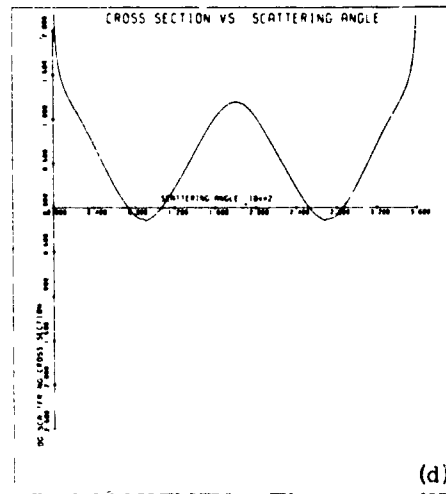
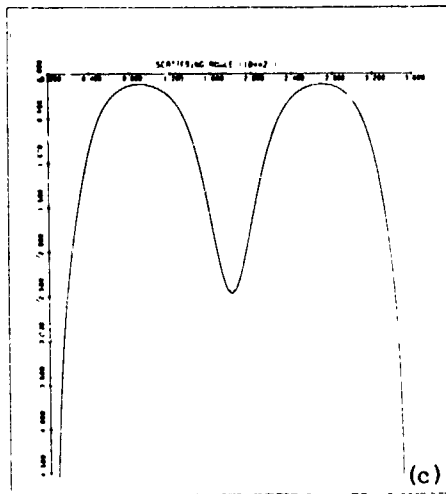
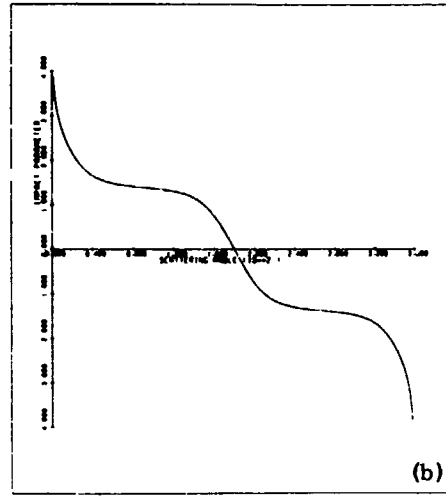
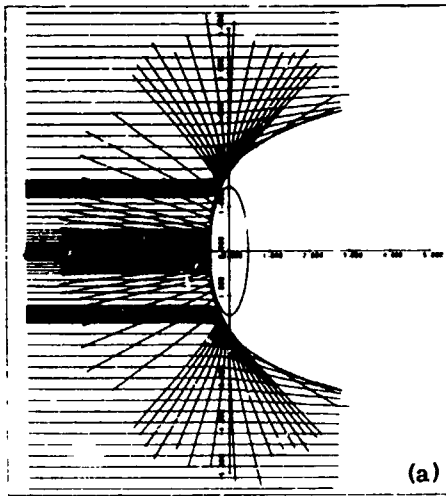


Figure 4. Scattering From an Elliptic Cylinder with $\rho = 2.0$, $R_o = 3$, and $\theta_R = 90^\circ$;
 (a) Ray Paths, (b) b vs θ , (c) $db/d\theta$, (d) $\sigma(\theta)$

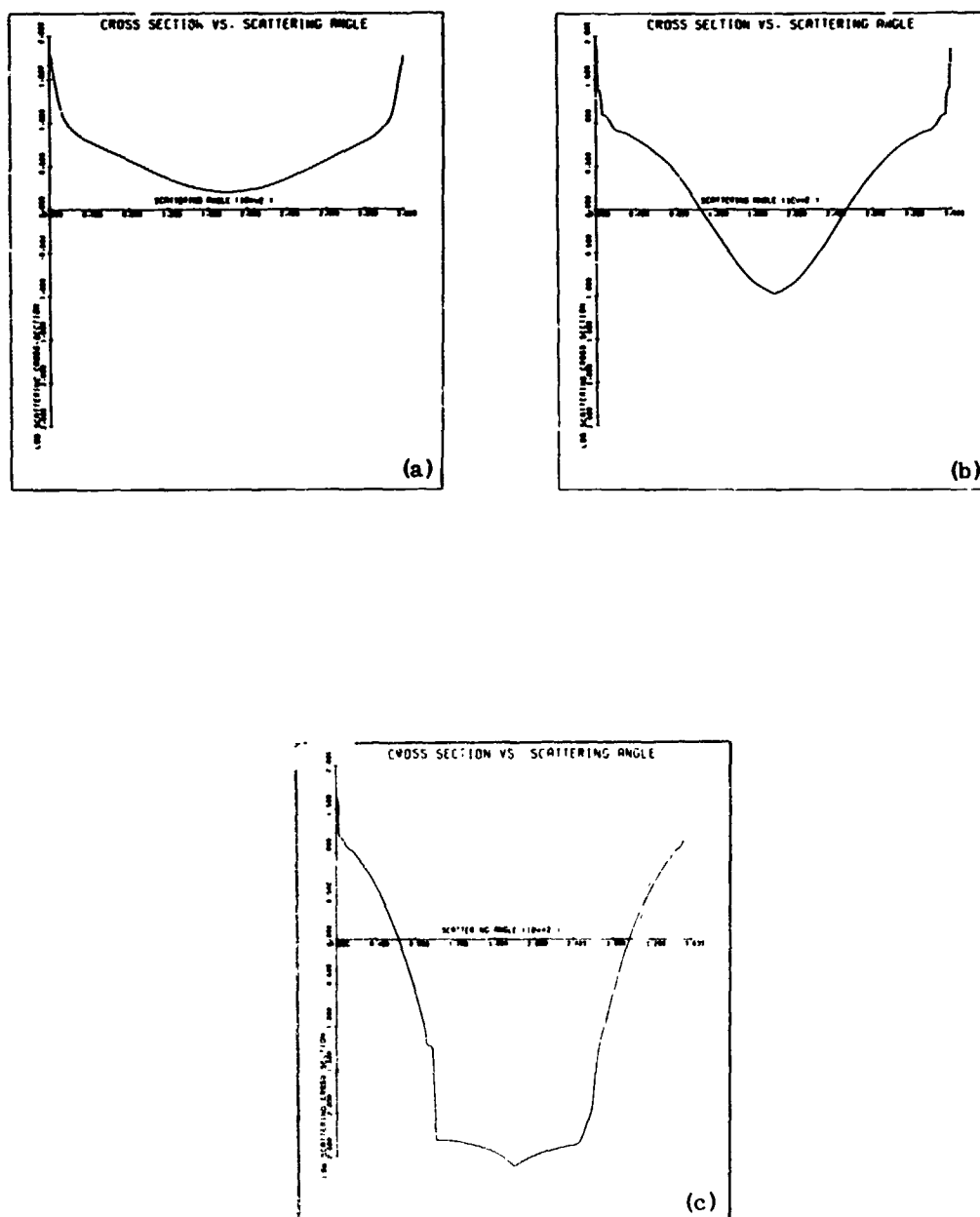


Figure 5. Differential Cross Section for $\rho = 2.0$, $\theta_R = 0^\circ$, and Several Values of R_0 ; (a) $R_0 = 1$, (b) $R_0 = 2$, (c) $R_0 = 5$

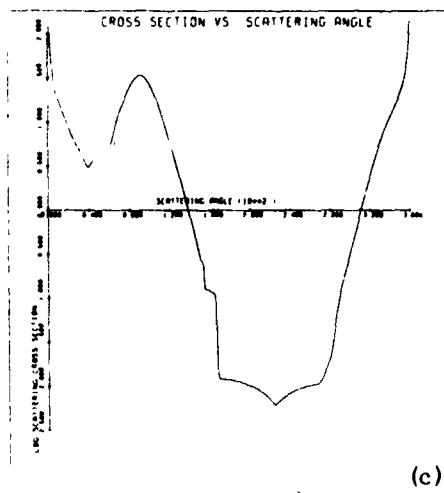
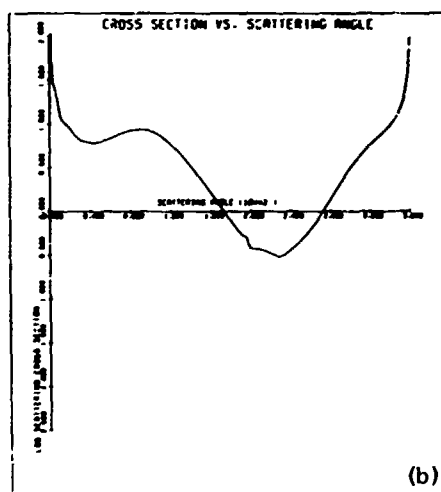
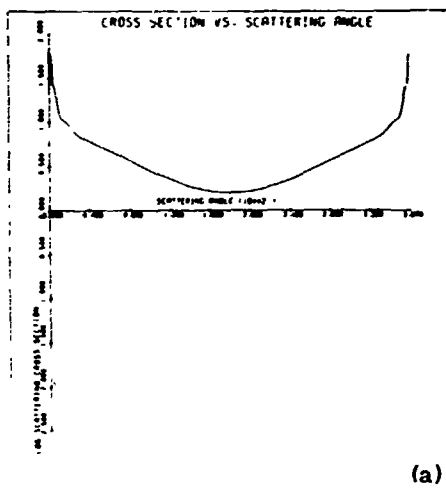


Figure 6. Differential Cross Section for $\rho = 2.0$, $\theta_R = 45^\circ$, and Several Values of R_0 :
 (a) $R_0 = 1$, (b) $R_0 = 2$, (c) $R_0 = 5$

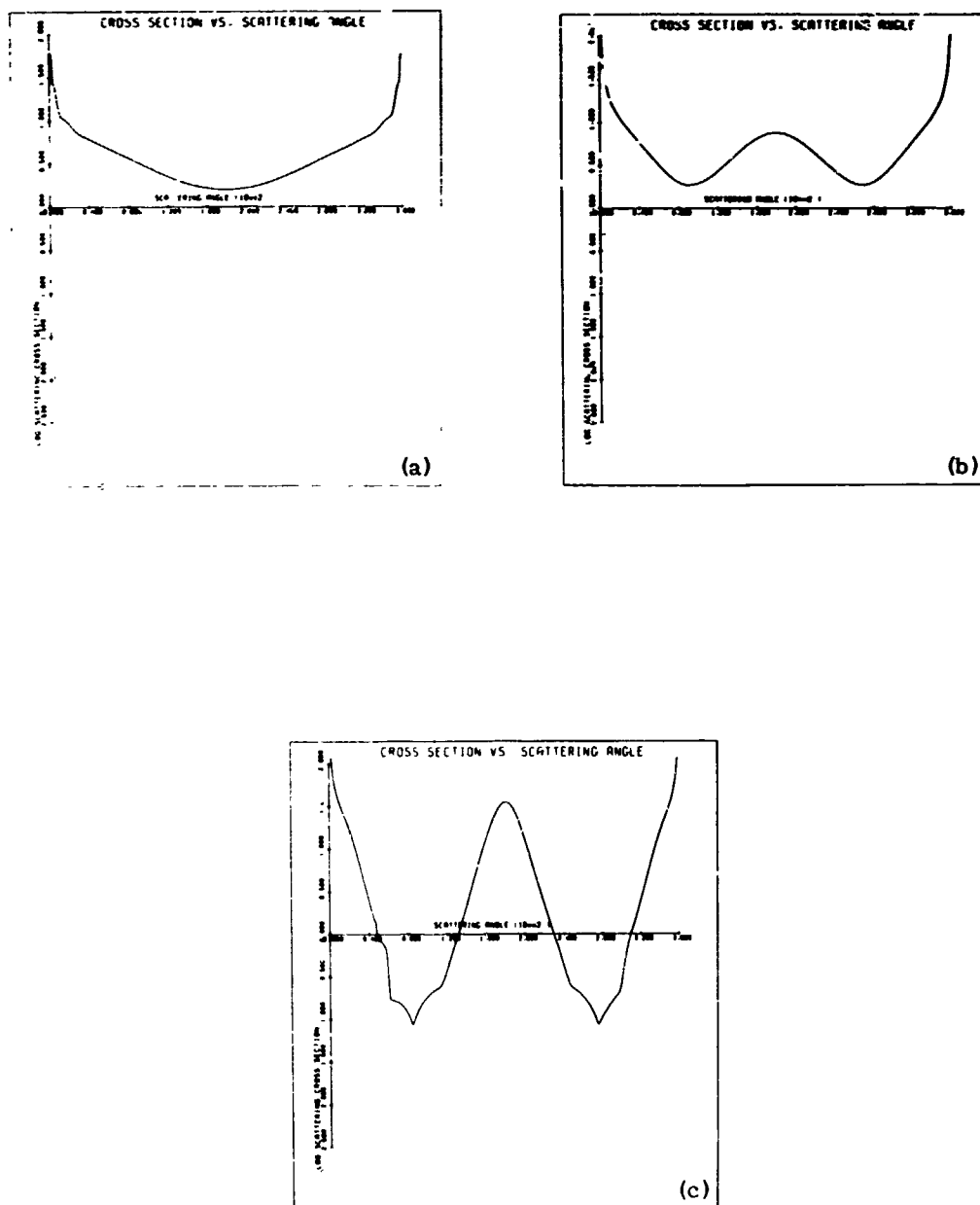


Figure 7. Differential Cross Section for $\rho = 2.0$, $\theta_R = 90^\circ$, and Several Values of R_0 ; (a) $R_0 = 1$, (b) $R_0 = 2$, (c) $R_0 = 5$

In Figure 8 we have plotted the location of the peak vs the rotation angle of the ellipses for $R_0 = 2, 3$ and 5 . The points which do not lie on the line $\theta_{\max} = 2\theta_R$ probably are different due to the reflecting body being an ellipsoid.

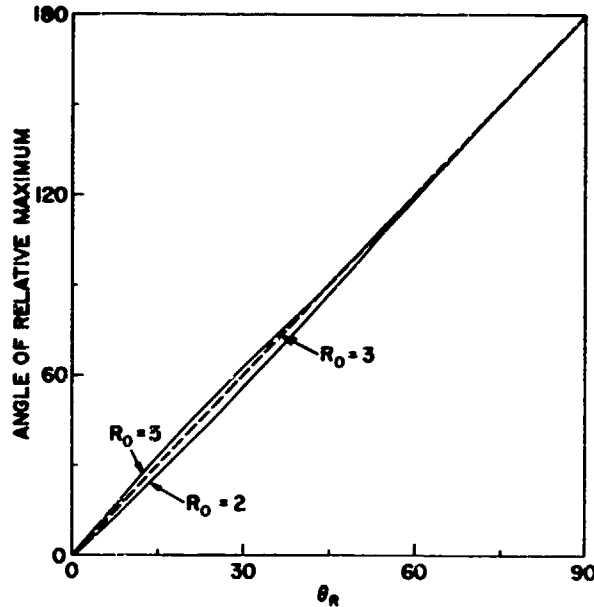


Figure 8. Angle of Relative Maximum of Differential Cross Section vs θ_R

In Figure 9 we have shown how the cross section at an orientation 0° , 45° and 90° changes as we vary ρ and keep $R_0 = 3$. One of the important features we have noted is the insensitivity of the total cross section to ρ . Figure 9 shows the variation in cross section is not very significant for ρ greater than 2.

In Figure 10 we have plotted the total cross section per unit length vs R_0 for four different angles of rotation. This graph demonstrates how elongation of the distribution can increase or decrease the total cross section; for an angle of about 20° , the cross section remains relatively constant regardless of the value of R_0 .

In Figure 11 we can see the large change in the total cross section as a function of angle. This graph demonstrates the importance of knowing how the ellipse is aligned in order to properly interpret radar data. In addition, we have also plotted the smooth data on this curve for $R_0 = 5$ to show how the total cross section has increased with the smoothing.

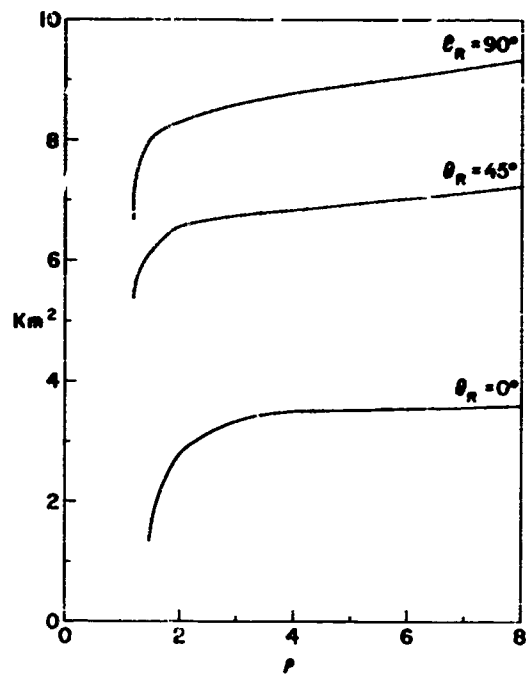


Figure 9. Total Cross Section vs ρ for $R_0 = 3$, and Several Values of θ_R

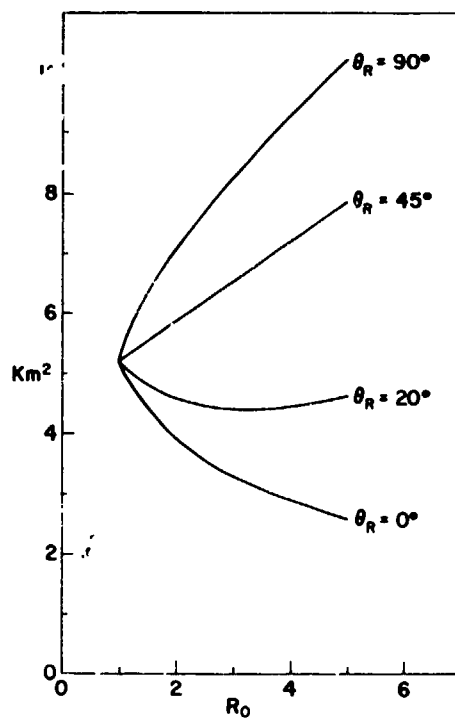


Figure 10. Total Cross Section vs R_0 for $\rho = 2.0$, and Several Values of θ_R

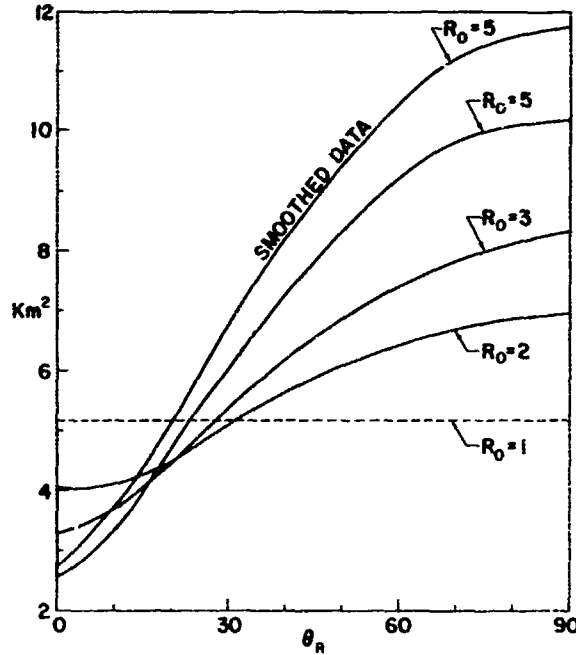


Figure 11. Total Cross Section vs θ_R for $\rho = 2.0$, and Several Values of R_0

5. RESULTS FOR THE PROLATE ELLIPSOID

In the case of a prolate ellipsoid, the cross section of the electron density distribution perpendicular to the major axis is a circle. If we have a plane wave incident along the major axis of the ellipse, it encounters a circularly symmetric charge distribution, and we can apply Eq. (1) to calculate the differential cross section.

In Figure 12 we show the differential cross section for $R_0 = 1, 2$ and 5 . From these curves it appears that elongating the distribution has an effect similar to decreasing the size of a spherical distribution or decreasing the value of ρ . If we integrate Eq. (1), we obtain the total cross section $\sigma = \frac{1}{4\pi} \int_0^{2\pi} \sigma(\theta) d\theta$ of the ellipsoid.

In Figure 13 we have plotted the total cross section vs R_0 keeping the total electron content constant. For this case Eq. (19) has to be modified such that z_0 is a function of the cube root of the ratio. From Figure 13 we can see the dramatic decrease in the total cross section as the incoming wave encounters a smaller area perpendicular to the direction of propagation and thus has a smaller backscatter region.

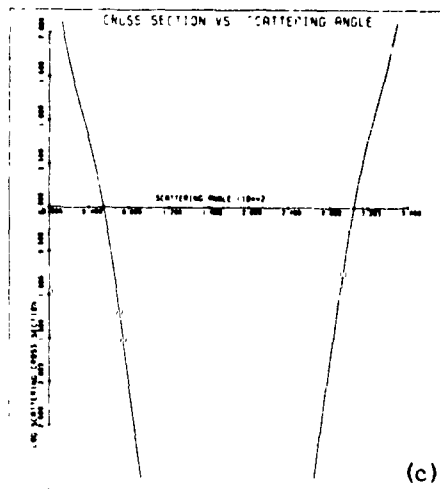
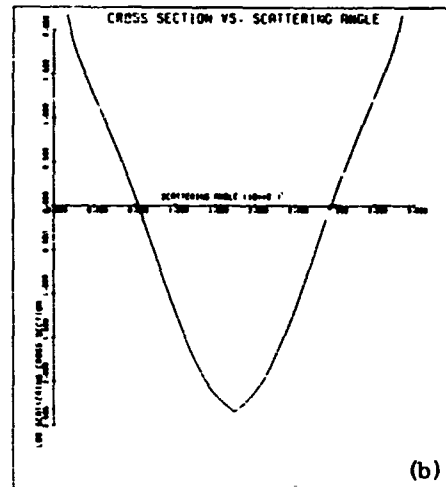
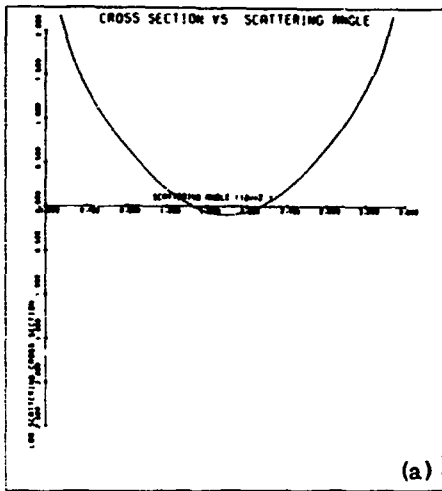


Figure 12. Differential Cross Section vs Scattering Angle with Azimuthal Symmetry, $\rho = 2.0$, $\theta_R = 0^\circ$ and Several Values of R_0 ; (a) $R_0 = 1$, (b) $R_0 = 2$, (c) $R_0 = 5$

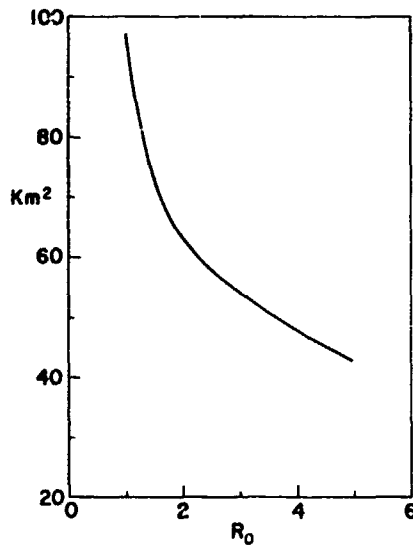


Figure 13. Total Cross Section of Ellipsoid vs R_0 for $\theta_R = 0^\circ$ and $\rho = 2.0$

6. RESULTS OF THE PROLATE ELLIPSOID IN A MAGNETIC FIELD

We have performed some scattering calculation for the case of a prolate ellipsoid with $\rho = 2.0$ with the magnetic field aligned along the major axis of the ellipse and a gyromagnetic ratio of 0.3. Calculations of the differential cross section for both ordinary and extraordinary rays with $R_0 = 1, 2$ and 5 are presented in Figures 14 and 15. The cross section for the ordinary ray has a somewhat lower cross section than that for no magnetic field. The cross section for the extraordinary ray is always higher than the nonmagnetic field results for $R_0 = 1$ but is, however, higher only near forward scatter for other values of R_0 .

7. COMPARISON OF GAUSSIAN AND CONDUCTING ELLIPSOIDS

To show the effect of a change from a continuous density distribution to the extreme case of a conducting body, we have plotted the scattering cross sections at $\theta_R = 0$ and $R_0 = 3$ of the Gaussian ellipsoid ($\rho = 2$) and the perfectly conducting ellipsoid (Crispin and Siegel, 1968). The surface of the conducting ellipsoid was chosen to correspond to the critical surface of the Gaussian ellipsoid. As indicated by Figure 16 the cross section for the Gaussian distribution is larger for a range of forward scattering angles but decreases so rapidly that it is

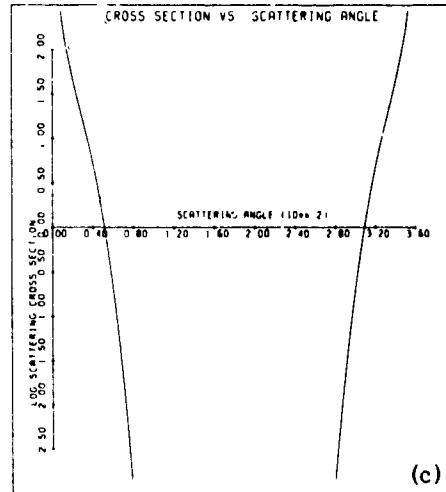
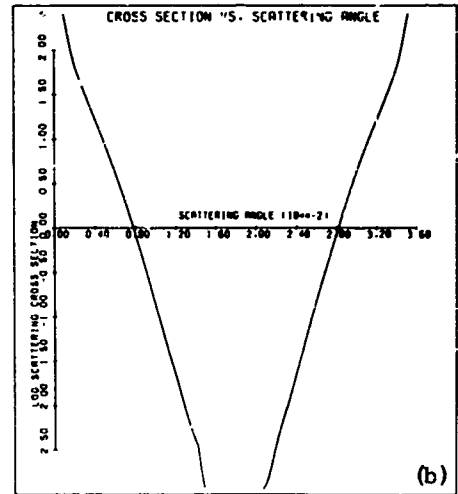
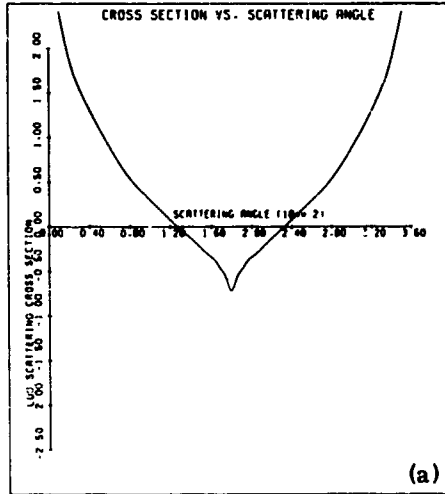


Figure 14. Differential Cross Section of Ordinary Ray vs Scattering Angle for $\rho = 2.0$, $\theta_R = 0^\circ$, and Several Values of R_0 ; (a) $R_0 = 1$, (b) $R_0 = 2$, (c) $R_0 = 5$

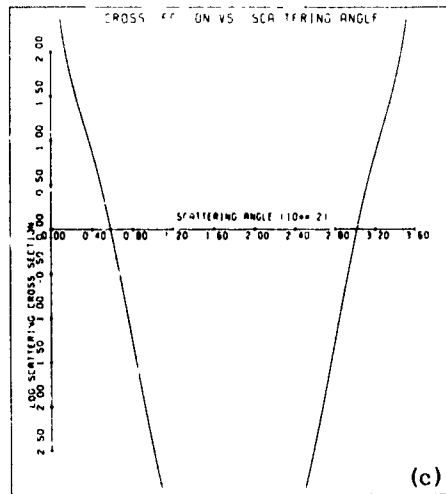
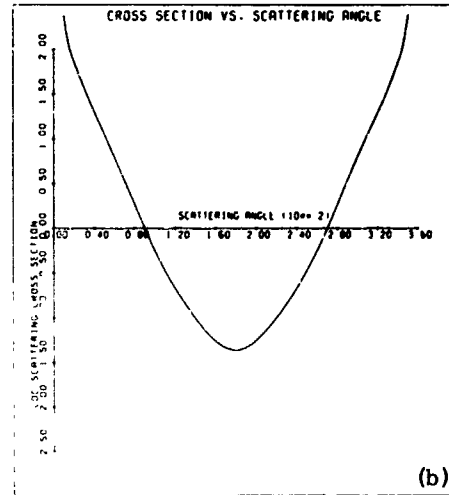
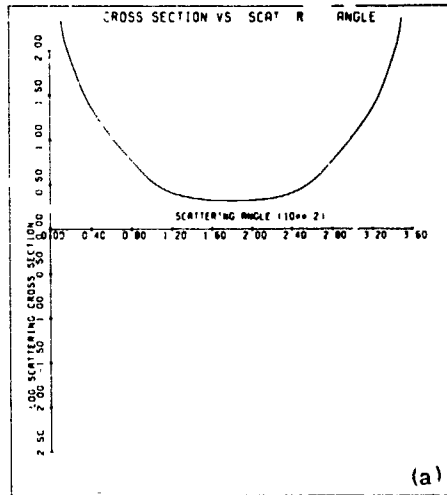


Figure 15. Differential Cross Section of Extraordinary Ray vs Scattering Angle for $\rho = 2.0$, $\theta_R = 0^\circ$, and Several Values of R_0 ; (a) $R_0 = 1$, (b) $R_0 = 2$, (c) $R_0 = 5$

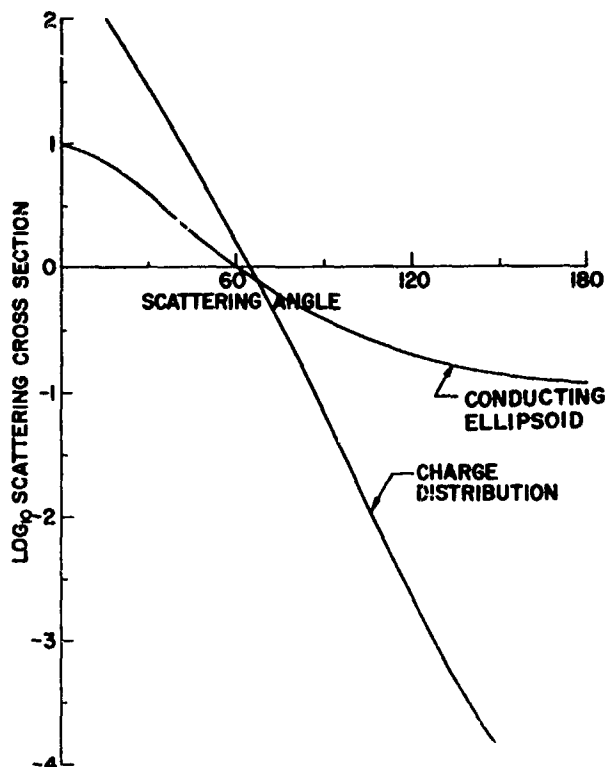


Figure 16. Comparison of Conducting Ellipsoid and Ellipsoidal Electron Density Distribution

considerably below the cross section of the conducting ellipsoid for the range of backward scattering angles. Similar results (not shown here) are obtained for the case of the elliptic cylinder with the incident ray along the major axis of the ellipse. These results corroborate previous work for the Gaussian sphere (Klein and Mabee, 1968), which indicates that the replacement of a moderately overdense Gaussian sphere by a conducting sphere of critical size is a poor approximation. In highly overdense bodies, however, the density gradient in the critical region is quite high so that here this approximation may be a reasonable one.

8. CONCLUDING REMARKS

It should now be obvious that the shape of an electron distribution and its orientation to an observer are very important in determining the differential and total cross section. Thus with the figures available in this report, it is hoped that cross section values of charge distributions can be approximated by properly applying the data presented and taking care of end effects for finite length cylinders.

We have shown that the magnetic field decreases slightly the differential cross section for the ordinary ray, but the extraordinary ray has a larger cross section than the same charge distribution when we do not have a magnetic field. We have indicated the error involved by trying to replace a charge distribution by a conducting body. The characteristic differential cross sections are so different that we could only use a conducting body for a very small range of scattering angles. Although the computer code in Appendix A was written for a CDC 6600, it should be easily converted to another system with minimal effort so that individual cases could be calculated. In addition, subroutine DERIV is written for a Gaussian charge distribution. If another charge distribution were desired, only this subroutine would be affected.

Appendix A

Computer Code for Ellipsoidal Scattering

```

PROGRAM ELLIPOS(INPUT,OUTPUT,TAPE5=INPUT,TAPE6=OUTPUT,TAPE3,
1TAPE2)
EXTERNAL DEPIV,OUTP
COMMON X(300),Z(300),ALPHA(300),ICOUNT
COMMON B(100),SCATAV(100)
DIMENSION XLABEL(3),YLABEL(3),TITLE(8),YLAB(3),XX(2),YY(2),TITL(8)
DIMENSION PRNT(3),Y(3),DERV(3)
DIMENSION XLABL(3),YLABL(3),FACTOR(10)
DIMENSION DISP_(2),DUMY(2),ANGI(2),RAY(2,2)
C
C THE FOLLOWING ARRAYS DEPEND ON THE NUMBER OF
C INTERPOLATED POINTS
C
COMMON ANGIPT(360),PTNT(360),DRDA(360),STGL(360),SORDA(360)
COMMON/CONST/ RHO,X0,Z0,THETA,THETAH,YYY,II
DATA (RAY(K,1),K=1,2)/20H ORDINARY RAY /
DATA (RAY(K,2),K=1,2)/20H EXTRAORDINARY RAY /
DATA TITL/8*10H /
DATA TITL/34HCRSS SECTION VS. SCATTERING ANGLE /
DATA XLABL,YLABL/6*10H /
DATA XLABEL/30H SCATTERING ANGLE/
DATA YLABL/30HIMPACT PARAMETER /
PI=3.1415926535896
RAD=PI/180.
ITITL=1
ITL=34
XSIZE=11.0
YSIZE=11.0
IPAGE=0
C
C II= 1 FOR THE ORDINARY RAY
C II = 2 FOR THE EXTRAORDINARY RAY
C
C ITIME = THE NUMBER OF CASES TO BE RUN.
C
DO 501 ITIME=1,4
C
C READ IN HARDNESS, MAJOR AND MINOR AXIS, AND INCLINATION OF
C ELLIPSOID
C
READ(5,10) RHO,X0,Z0,THETA
10 FORMAT (4F10.0)
READ(5,10) THETAH,YYY
C
C III IS THE NUMBER OF ORIENTATIONS PER CASE.
C
DO 61 III=1,2
II=III
THETA=THETAH
N?=359

```



```

IF (THETA.EQ.0.0.OR.THETA.EQ.90.0) GO TO 25
INDM=55-INT(X*(PI/2.))
AVG=130.-THETA
AMX=(7*(INDM)-7*(INDM-1))/(X(INDM)-X(INDM-1))
DO 31 I=1,50
IND=(ANG+2.*ELJAT(I))/2.
AM1=(7*(IND)-7*(IND-1))/(X(IND)-X(IND-1))
IF (AM1.GT.AMX) INDM=IND
IF (AM1.GT.A4X) AMX=AM1
31 CONTINUE
DATA FACTOR/0.010,0.025,0.050,0.10,0.25,0.50,1.0,2.0,5.0/
25 DO 41 I=1,100
R(I)=0.0
41 CONTINUE
ZERO=7*(INDM)+0.3*AM7*SIN(-2.0*THETA*RAD)
IF (THETA.EQ.0.0.OR.THETA.EQ.90.0) ZERO=0.0
AM7Z=AM7
IF (AM7.LE.X0*CS(45.*RAD).AND.X0/Z0.GE.3) AM7=AM7*0.3
DO 71 I=1,49
R(50)=ZERO
J=8
IF (I.LE.25) J=7
IF (I.LE.22) J=5
IF (I.LE.18) J=5
IF (I.LE.15) J=4
IF (I.LE.12) J=3
IF (I.LE.8) J=2
IF (I.LE.4) J=1
DIF=FACTOR(J)*AM7
IF (DIF.GT.0.25) DIF=0.25
IF (R(51-I).LE.AM7Z.AND.DIF.GT.0.15) DIF=0.15
IF (R(51-I).GT.AM7Z-0.25.AND.R(51-I).LT.AM7Z+0.15
1.AND.THETA.EQ.30.) DIF=0.025
R(50-I)=R(51-I)+DIF
R(50+I)=R(49+I)-DIF
71 CONTINUE
J=0
DO 81 I=1,100
IF (R(I).EQ.0.0) GO TO 81
IF (ABS(R(I))) .GT.4.0*AM7Z) GO TO 81
J=J+1
R(J)=R(I)
81 CONTINUE
?
? IMP= NUMBER OF IMPACT PARAMETERS.
?
IMP=J
WRITE(6,50) (R(I),I=1,IMP)
50 FORMAT (//,27H THE IMPACT PARAMETERS ARE,/,10(10F10.3,/)
?
C START RAY TRACING.

```

```

C
DO 21 I=1,IMP
ICOUNT=0
C
C PRMT(3)= INITIAL STEP SIZE. IF IT IS NEGATIVE, EACH STEP
C IS NOT PRINTED
C PRMT(4)= MAXIMUM ANGULAR CHANGE PER STEP.
C
PRMT(3)=-0.25
PRMT(4)=PI/60.0
Y(1)=-5.0
Y(2)=9(I)
Y(3)=0.0
NDIM=3
IF (PRMT(3).LE.0.0) GO TO 35
IPAGE=IPAGE+1
WRITE(6,40) IPAGE
35 CALL RKGS(PRMT,Y,DERV,NDIM,IMLF,DERIV,OUTP)
C
C PLOT SCATTERED RAYS.
C
CALL PLOTV(2,X,XS,Z,YS,ICOUNT,33,1,ITITL,TITLE,XLABEL,YLABEL,
1XSIZE,YSIZE)
SCATAN(I)=ALPHA(ICOUNT)/RAD
IF (SCATAN(I).LT.0.0) SCATAN(I)=360.+SCATAN(I)
21 CONTINUE
C
C CHECK FOR ZERO SCATTERING AT NORMAL INCIDENCE.
C
IMP1=IMP
IE=0
DO 91 I=2,IMP
53 IF (SCATAN(I).GT.SCATAN(I-1)) GO TO 51
GO TO 52
51 IF (SCATAN(I+1).GT.SCATAN(I)) GO TO 92
52 IMP1=IMP1-1
DO 101 J=I,IMP1
SCATAN(J)=SCATAN(J+1)
R(J)=R(J+1)
101 CONTINUE
IF (I.GT.IMP1-1) GO TO 5
GO TO 53
32 IF (IE.NE.0) GO TO 91
IF (SCATAN(I).GT.180.) IE=I
91 CONTINUE
5 IMP=IMP1
DATA ANGI/180.,180.1/
CALL INTP(SCATAN,IE-2),R(IE-2),4,ANGI,DISPL,DUMY,2,JL,JH)
WRITE(6,100) DISPL(1)
100 FORMAT (/,30X,* DISPLACEMENT = *F6.3)
C

```

```

C
C WRITE INPUT PARAMETERS, IMPACT PARAMETERS, AND SCATTERING
C ANGLES ON TAPE2.
C
WRITE(2,70) R40,X0,Z0,THETA,THETAH,YYY,DDATE,IMP
70 FORMAT(5F10.5,4I0,I10)
WRITE(2,80) (R(I),SCATAN(I),I=1,IMP)
80 FORMAT (8F10.5)
C
C CONVERT SCATTERING ANGLE TO RADIAN AND INTERPOLATE  $\theta$  VS.
C SCATTERING ANGLE.
C
DO 131 I=1,IMP
R(I)=R(I)-DISP_(1)
SCATAN(I)=SCATAN(I)*RAD
131 CONTINUE
DT=2.0*PI/360.
ANGINT(1)=0.001/57.*DT
DO 221 I=2,NP
ANGINT(I)=ANGINT(I-1)+DT
221 CONTINUE
CALL INTP(SCATAN,B,IMP,ANGINT,RINT,ORDA,NP,JL,JH)
DO 141 I=JL,JH
ANGINT(I-JL+1)=ANGINT(I)/RAD
RINT(I-JL+1)=RINT(I)
ORDA(I-JL+1)=ORDA(I)
141 CONTINUE
NP=JH-JL+1
C
C PLOT IMPACT PARAMETERS VS. SCATTERING ANGLE.
C
XX(1)=0.0
XX(2)=360.0
YY(1)=-3.0
YY(2)=3.0
SX=40.
SY=1.0
CALL PLOTV(3,XX,40.,YY,1.0,2,33,-1,ITITL,TITLE,XLABEL,YLABEL,
1,XSIZE,YSIZE)
CALL PLOTV(2,ANGINT,40.,RINT,1.0,NP,33,1,ITITL,TITLE,XLABEL,YLABEL
1,XSIZE,YSIZE)
C
C SMOOTH DERIVATIVES
C
IFILTR=5
NP1=NP-1
DO 201 NSM=1,1
IF(NSM.EQ.1) GO TO 45
DO 181 J=2,NP1
IJ=IFILTR
IF(J.LE.IFILTR-1) IJ=J-1
IF(J+IFILTR.GE.NP) IJ=NP-J

```

```

SDBDA(J)=0.0
DO 191 J=1,IJ
SDBDA(J)=SDBDA(J)+DBDA(J+JJ)+DBDA(J-JJ)
191 CONTINUE
SDBDA(J)=SDBDA(J)+DBDA(J)
SDBDA(J)=SDBDA(J)/ELCST(2*IJ+1)
191 CONTINUE
DO 171 J=2,NP
DBDA(J)=SDBDA(J)
171 CONTINUE
IF(NSM.EQ.2) GO TO 201

C
C   CALCULATE CROSS SECTION
C
45 SUM=0.0
DO 121 I=1,NP
SIGL(I)=4.0*PI*DBDA(I)*DBDA(I)/SIN(ANGINT(I)*RAD)
121 CONTINUE
DO 111 I=1,NP
SC=1.0
IF(I.EQ.1.OR.I.EQ.NP) SC=0.5
SUM=ABS(SIGL(I))*SC+SUM
SIGL(I)=ALOG10(ABS(SIGL(I)))
111 CONTINUE
SUM=SUM+0.5*(+ANGINT(1))*(DBDA(1)*(-ANGINT(1))+10.**SIGL(1))
SUM=SUM+0.5*(350.-ANGINT(NP))*(DBDA(NP)*(ANGINT(NP)-360.)+10.**
1SIGL(NP))
SUM=SUM*RAD
WRITE(6,120) SUM
120 FORMAT (///,30X,'TOTAL CROSS SECTION =*EJ,3.84 (KM**2)')
IPAGE=IPAGE+1
WRITE(6,40) IPAGE
L=NP/100+1
DO 151 K=1,L
LL=(K-1)*100+1
LU=K*100
IF(K.EQ.L) LU=NP
WRITE(6,90)
90 FORMAT (2,' SCATTERING ANGLE   IMPACT PARAMETER   DERIVATIVE   _ (
1G SIGMA*,5X)
WRITE(6,170) (ANGINT(I),RINT(I),DBDA(I),SIGL(I),I=LL,LU)
170 FORMAT (2(5X,F7.2,13X,F5.3,13X,F7.4,5X,F6.3,6X))
IPAGE=IPAGE+1
WRITE(6,40) IPAGE
151 CONTINUE
XX(1)=0.0
XX(2)=760.0
YY(1)=0.0
YY(2)=-4.0
SY=0.5
CALL PLOTV(3,XX,SX,YY,SY,2,33,-1,ITITL,TITLE,XLABEL,YLABEL,XSIZE,

```

```
1YSIZE)  
CALL PLOTV(2,ANGINT,SX,ORQA,SY,NO,33,1,ITTL,TITLE,XSIZE,YSIZE,  
1XSIZE,YSIZE)  
XX(1)=0.0  
XX(2)=360.0  
YY(1)=2.0  
YY(2)=-2.50  
SY=0.50  
DATA YLAB/30HL06 SCATTERING CROSS SECTION /  
CALL PLOTV(3,XX,SX,YY,SY,2,33,-1,ITL,ITTL,XLABEL,YLAB,  
1XSIZE,YSIZE)  
CALL PLOTV(2,ANGINT,SX,SIGL,SY,NO,33,1,ITL,ITTL,XLABEL,YLAB,  
1XSIZE,YSIZE)  
201 CONTINUE  
51 CONTINUE  
501 CONTINUE  
ENDFILE 2  
CALL PLOTV(4)  
STOP  
END
```

```

SUBROUTINE DERI(YV,DERV,NEG)
C
C THIS SUBROUTINE CALCULATES THE DERIVATIVES OF AN ELLIPSOIDAL
C CHARGE DISTRIBUTION FOR THE RUNGE-KUTTA METHOD.
C
COMMON/CONST/ RHO,X0,Z0,THETA,THETAH,Y,I
DIMENSION W(2),QWDA(2),YY(3),DERV(3),DUDX(2),DUDZ(2)
PI=3.14159265
RAD=PI/180.
NEG=J
COST=COS(THETA*RAD)
SINT=SIN(THETA*RAD)
CHI=PHO*EXP(-((YY(1)*COST+YY(2)*SINT)/X0)**2
1-((-YY(1)*SINT+YY(2)*COST)/Z0)**2)
YL=Y*COS((-THETAH*RAD)+YY(3))
YT=Y*SIN((-THETAH*RAD)+YY(3))
W1=(YT**4)/4.+(YL**2)*((1.-CHI)**2)
IF(W1.LT.0.0) GO TO 5
W1=SQRT(W1)
W(1)=1.-CHI-(YT**2)/2.+W1
W(2)=1.-CHI-(YT**2)/2.-W1
AMU=1.-CHI*(1.-CHI)/W(I)
IF(AMU.LT.0.0) GO TO 5
IF(W1.EQ.0.) QWDA=0.0
IF(W1.EQ.0.) GO TO 35
QWDA(1)=YL*YT*(-1.+(YT**2-2.*(1.-CHI)**2)/(2.*W1))
QWDA(2)=YL*YT*(-1.-(YT**2-2.*(1.-CHI)**2)/(2.*W1))
QWDA=CHI*(1.-CHI)*QWDA(I)/(2.*SQRT(AMU)*W(I)**2)
35 CONTINUE
DCHI1X=-2.*CHI*(YY(1)*COST+YY(2)*SINT)*COST/(X0**2)
1-(-SINT*YY(1)+YY(2)*COST)*SINT/(Z0**2)
DCHI1Z=-2.*CHI*(YY(1)*COST+YY(2)*SINT)*SINT/(X0**2)
1+(-YY(1)*SINT+YY(2)*COST)*COST/(Z0**2)
IF(W1.EQ.0.0) GO TO 45
DUDX(1)=DCHI1X*(2.*CHI-1.-CHI*(1.-CHI)*(1.+(1.-CHI)*(YL**2)/
1W1)/W(I))/(2.*SQRT(AMU)*W(I))
DUDX(2)=DCHI1X*(2.*CHI-1.-CHI*(1.-CHI)*(1.-(1.-CHI)*(YL**2)/
1W1)/W(I))/(2.*SQRT(AMU)*W(I))
DUDZ(1)=DCHI1Z*(2.*CHI-1.-CHI*(1.-CHI)*(1.+(1.-CHI)*(YL**2)/
1W1)/W(I))/(2.*SQRT(AMU)*W(I))
DUDZ(2)=DCHI1Z*(2.*CHI-1.-CHI*(1.-CHI)*(1.-(1.-CHI)*(YL**2)/
1W1)/W(I))/(2.*SQRT(AMU)*W(I))
GO TO 55
45 DUDX(1)=-DCHI1X/(2.*SQRT(AMU))
DUDX(2)=-DCHI1Z/(2.*SQRT(AMU))
DUDZ(1)=-DCHI1Z/(2.*SQRT(AMU))
DUDZ(2)=-DCHI1Z/(2.*SQRT(AMU))
55 YY3=YY(3)
DXDT=(SQRT(AMU)*COS(YY3)+QWDA*SIN(YY3))/AMU
DZDT=(SQRT(AMU)*SIN(YY3)-QWDA*COS(YY3))/AMU
DADT=(COS(YY3)*DUDZ(I)-SIN(YY3)*DUDX(I))/AMU

GO TO 15
5 NEG=-1
GO TO 25
15 DERY(1)=DXDT
DERV(2)=DZDT
DERV(3)=DADT
25 CONTINUE
RETURN
END

```

```

SUBROUTINE OUTP (XX, Y, DERY, IHLF, PRMT, NEG)
  THIS SUBROUTINE PRINTS THE RESULTS OF THE RUNGE-KUTTA INTEGRATION
  AND DETERMINES WHEN WE HAVE FOLLOWED A RAY FAR ENOUGH.

  DIMENSION Y(3), DERY(3), PRMT(5)
  IF (DERY(3) .LT. 1.0E-5 .AND. XX .GT. 8.0) PRMT(5) = -1.0
  IF (PRMT(3) .LT. 0.0) GO TO 5
  WRITE(6,10) XX, (Y(J), J=1,3), (DERY(J), J=1,3), IHLF, NEG
10  FORMAT (7E17.8,2I5)
  RETURN
END

SUBROUTINE RKGS (PRMT, YY, DERY, NDIM, IHLF, DERIV, OUTP)
  THIS SUBROUTINE PERFORMS THE RUNGE-KUTTA INTEGRATION.

  DIMENSION PRMT(1), YY(1), DERY(1), X1(300), Y(300), ALPHA(300), <(3,4)
  DIMENSION XX(300), DADT(4)
  REAL K
  COMMON X1, Z, A1, A4, J
  COMMON /CONST/ R40, X0, Z0, THETA, THETAH, YYY, III

  SET UP THE INITIAL CONDITIONS.

  PI=3.14159265
  RAD=PI/180.
  THET=THETAH
  IF (ABS(THETAH) .GT. 90.) THET=180.-ABS(THETAH)
  THET=THET*PI
  IV0=0
  J=0
  DADT1=0.0
  IHLF=0
  X=0.0
  Y=ABS(PRMT(3))
  ERR=PRMT(4)
  PRMT(5)=0.0
35  J=J+1
  IF (J .GE. 300) WRITE(6,10)
10  FORMAT (//,20X, *THE NUMBER OF STEPS HAS EXCEEDED THE DIMENSION*)
  IF (J .GE. 300) GO TO 55
  X1(J)=YY(1)
  Y(J)=YY(2)
  ALPHA(J)=YY(3)
  XX(J)=Y
45  II=0

  CALCULATE THE DERIVATIVES, AND CHECK THAT NO ERROR HAS OCCURRED
  IN DERY.

  CALL DERIV(YY, DERY, NEG)
  CALL OUTP(X, YY, DERY, IHLF, PRMT, NEG)
  IF (PRMT(5) .NE. 0.0) GO TO 55
  II=II+1
  IF (IABS(NEG) .GT. 0) GO TO 15

```

```

3   STORE CONSTANTS AND CALCULATE THE NEXT SE OF VALUES AT WHICH
C   DERIVATIVES ARE REQUIRED.
?
    75 DO 21 I=1,NDIM
      K(I,II)=DERV(I)*H
    21 CONTINUE
      DADT(II)=DERV(3)

      IF(II.EQ.4) GO TO 25
      C=2.
      IF(II.EQ.3) J=1.
      YY(1)=X1(J)+K(1,II)/C
      YY(2)=7(J)+K(2,II)/C
      YY(3)=ALPHA(J)+K(3,II)/C
      X=XX(J)+H/C
      GO TO 5

3   DECREASE INTERVAL BY .5 IF AN ERROR HAS OCCURED IN CALCULATING
C   THE DERIVATIVES.
?
    15 H=H/2.
      IHLF=IHLF+1
      IF(IHLF.GT.40) GO TO 55
      IF(II.LE.2) J=J-1
      X=XX(J)
      YY(1)=Y1(J)
      YY(2)=7(J)
      YY(3)=ALPHA(J)
      GO TO 45

3   CALCULATE THE VALUE OF THE FUNCTION USING THE FOUR PREVIOUSLY
C   CALCULATED POINTS.
?
    25 DELX=(K(1,1)+2.*(K(1,2)+K(1,3))+K(1,4))/6.
      DELZ=(K(2,1)+2.*(K(2,2)+K(2,3))+K(2,4))/6.
      DELA=(K(3,1)+2.*(K(3,2)+K(3,3))+K(3,4))/6.
      DADT2=ABS((DADT(1)+DADT(2)+DADT(3)+DADT(4))/4.)

3   CHECK THAT THE ANGULAR CHANGE IS NOT GREATER THAN DESIRED.
C
      IF(ABS(DELA).GT.ERR) GO TO 15

3   STORE ACCEPTABLE VALUES OF THE INTEGRATION.
C
      YY(1)=X1(J)+DELX
      YY(2)=7(J)+DELZ
      YY(3)=ALPHA(J)+DELA
      X=XX(J)+H

3   CHECK FOR SPITZE CONDITION
C
      IF(YYY.EQ.0.0) GO TO 11
      IF(RHO.LT.1.0) GO TO 11
      IF(IND.EQ.1) GO TO 11
      RCR=SQRT(ALOG(RHO))
      IF(YY(1)**2+YY(2)**2-RCR.GT.1.0E-5) GO TO 11
      IF(ABS(YY(3)).LT.ABS(THET)) ER=(ABS(YY(3))-ABS(THET))*2.
      IF(ABS(YY(3)).GT.ABS(THET)) ER=(ABS(YY(3))-ABS(THET)-PI/2.)*2.0

```

```
C PHASE ANGLE MUST BE WITHIN 0.25 DEGREES OF THE MAGNETIC FIELD.  
C  
IF (ABS(ER).GT.RAD*.20) GO TO 11  
YY(3)=YY(3)+SIGN(E2,YY(3))  
IND=1  
C  
C CHECK IF THE INTERVAL OF INTEGRATION CAN BE INCREASED.  
C  
11 IF (ABS(DELA).LT.0.01.AND.DADT2.LT.DADT1) GO TO 65  
DADT1=DADT2  
GO TO 34  
65 DADT1=DADT2  
IF (H.GT.ABS(PRYT(3))) GO TO 35  
H=H*2.  
IHLF=IHLF-1  
GO TO 35  
95 RETURN  
END
```

Sample Data

2.0	1.000 0.30	1.000	0.0
2.0	1.587 0.30	0.794	0.0
2.0 0.0	2.080 0.3	0.693	
2.0	2.924 0.30	0.585	0.0

References

- Ahlberg, J.H., Nilson, E.N., and Walsh, J.L. (1967) Theory of Splines and Their Applications, Academic Press.
- Bates, Howard F., (1971) HF backscatter from high latitude ionospheric barium releases, Radio Science 6(No.1):21-23.
- Crispin, J.W., and Siegel, K.M. (1968) Methods of Radar Cross Section Analysis, Academic Press.
- Kelso, John M. (1964) Radio Ray Propagation in the Ionosphere, McGraw-Hill.
- Klein, Milton M., and Mabee, R.S. (1969) Scattering of HF Radio Waves by a Spherical Electron Cloud, AFCRL-69-0261.
- Klein, Milton M., and Rosenberg, N.W. (1971) Scattering of HF Radio Waves by a Spherical Electron Cloud in the Presence of a Magnetic Field, AFCRL-71-0371.
- Merzbacher, Eugen (1961) Quantum Mechanics, John Wiley and Sons, Inc.
- Rao, Pendyala B., Michael, A.E., and Thome, G.D. (1971) Ray Tracing Synthesis of HF Radar Signatures from Gaussian Plasma Clouds, Raytheon Company.
- Rosenberg, N.W. (1971) Private Communication.
- Scarborough, J.B. (1930) Numerical Mathematical Analysis, John Hopkins Press.
- Thome, G.D. (1969) Raytheon SECEDE III Radar Observations: A Preliminary Report, RADC-TR-69-239, 1:115-132.